Stellar populations across the ngc 4244 truncated galactic disk — **Source link** ↗

Roelof S. de Jong, Anil C. Seth, D. J. Radburn-Smith, Eric F. Bell ...+11 more authors

Institutions: Space Telescope Science Institute, Harvard University, Max Planck Society, University of California, Irvine ...+4 more institutions

Topics: Elliptical galaxy, Hubble sequence, Disc, Surface brightness fluctuation and Stellar density

Related papers:

- Stellar populations across the NGC4244 truncated galactic disk

- Beyond inside-out growth : formation and evolution of disk outskirts

- The structure of galactic disks - Studying late-type spiral galaxies using SDSS

- Radial mixing in galactic discs

- The secular evolution of disk structural parameters

Share this paper: ☍ ✉ ⓵ ✉

View more about this paper here: https://typeset.io/papers/stellar-populations-across-the-ngc-4244-truncated-galactic-2yiufu1u2b

9-2007

Stellar populations across the NGC 4244 truncated galactic disk.

Roelof de Jong
Space Telescope Science Institute

A. C. Seth
Harvard-Smithsonian Center for Astrophysics

D. Radburn-Smith
Space Telescope Science Institute

E. F. Bell
Max-Planck-Institut fur Astronomie

T. M. Brown
Space Telescope Science Institute

See next page for additional authors

Original Publication Information

Authors

Roelof de Jong, A. C. Seth, D. Radburn-Smith, E. F. Bell, T. M. Brown, J. S. Bullock, S. Courteau, J. J. Dalcanton, H. C. Ferguson, P. Goudfrooij, S. Holfeltz, Benne W. Holwerda, C. Purcell, J. Sick, and D. B. Zucker

STELLAR POPULATIONS ACROSS THE NGC 4244 TRUNCATED GALACTIC DISK

Roelof S. de Jong,[1] A. C. Seth,[2] D. J. Radburn-Smith,[1] E. F. Bell,[3] T. M. Brown,[1] J. S. Bullock,[4] S. Courteau,[5]
J. J. Dalcanton,[6] H. C. Ferguson,[1] P. Goudfrooij,[1] S. Holfeltz,[1] B. W. Holwerda,[1]
C. Purcell,[4] J. Sick,[7] and D. B. Zucker[8]

ABSTRACT

We use the *Hubble Space Telescope* ACS to study the resolved stellar populations of the nearby, nearly edge-on galaxy NGC 4244 across its outer disk surface density break. The stellar photometry allows us to study the distribution of different stellar populations and reach very low equivalent surface brightnesses. We find that the break occurs at the same radius for young, intermediate-age, and old stars. The stellar density beyond the break drops sharply by a factor of at least 600 in 5 kpc. The break occurs at the same radius independent of height above the disk, but is sharpest in the midplane and nearly disappears at large heights. These results make it unlikely that truncations are caused by a star formation threshold alone: the threshold would have to keep the same radial position from less than 100 Myr to 10 Gyr ago, in spite of potential disturbances such as infall and redistribution of gas by internal processes. A dynamical interpretation of truncation formation is more likely, such as due to angular momentum redistribution by bars or density waves, or heating and stripping of stars caused by the bombardment of dark matter subhalos. The latter explanation is also in quantitative agreement with the small diffuse component we see around the galaxy.

Subject headings: galaxies: evolution — galaxies: halos — galaxies: individual (NGC 4244) —
galaxies: spiral — galaxies: stellar content — galaxies: structure

1. INTRODUCTION

Using photographic plates of edge-on galaxies, van der Kruit (1979) was the first to note that some spiral galaxies have truncated disks. More recent studies with CCDs of galaxies at a range of inclinations have found that these truncations are not the end of the stellar disk, but are better described as a change in the exponential length scale of the radial light distribution (Pohlen et al. 2002). These downward breaks in the light profile occur in the majority of galaxies (Pohlen & Trujillo 2006). Many different models have been proposed to explain the truncations or breaks but they can all be placed into two broad categories: models that form stars in the observed configuration, and models that transport stars into the observed configuration by dynamical effects. Here we use observations of the resolved stellar populations of the edge-on galaxy NGC 4244 to constrain these types of models.

The observed projection of a galaxy can affect the detectability of breaks in the light profiles. Breaks were originally discovered using edge-on galaxies (van der Kruit 1979; van der Kruit & Searle 1981) and seem to be more readily observed in edge-on galaxies than face-on galaxies. This can be partly explained by the line-of-sight projection that allows one to probe fainter (deprojected) surface brightnesses for edge-on galaxies. Furthermore, to reach faint isophotes in face-on galaxies, azimuthal smoothing is used to extract radial profiles. This technique, however, smooths out the nonaxisymmetric features (bars, spiral arms) that could result in sharp features in edge-on projections.

A number of recent studies with larger samples of galaxies

have tried to bridge the projection gap and have identified a number of characteristics of breaks. Erwin et al. (2005) and Pohlen & Trujillo (2006) identify three types of luminosity profiles: those with a decreasing scale length beyond the break, those with an increasing scale length, and those with no break at all. Downward breaks generally occur at 2–4 disk scale lengths, with galaxies at the short end of that range typically exhibiting lower central surface brightnesses and larger scale lengths. These correlations cause the breaks to occur at a similar surface brightness in different galaxies (Kregel & van der Kruit 2004). The breaks occur at about the same radius independent of the height above the midplane (Pohlen et al. 2007), and appear to be present already at redshifts $z \sim 1$ (Pérez 2004; Trujillo & Pohlen 2005). There are some indications that disk breaks and (gaseous) warps are related, but there are exceptions to the rule (van der Kruit 2007).

As mentioned earlier, models to explain the downward breaks in galaxy disks come in two broad categories. In the first group the breaks are created by stars forming intrinsically in the observed distribution, as a result of either a limit in the gas distribution (van der Kruit 1987), or some kind of threshold suppressing star formation (e.g., Fall & Efstathiou 1980; Kennicutt 1989; Schaye 2004; Elmegreen & Hunter 2006). In the second category are models that rearrange the stars after they form. This may occur by redistribution of angular momentum due to bars and spiral arms (e.g., Debattista et al. 2006; K. Foyle et al. 2007, in preparation), or by the stripping of stars due to repeated tidal interaction with other galaxies (e.g., Gnedin 2003) or dark matter subhalos (Kazantzidis et al. 2007).

To constrain the large number of models in the literature we investigate the resolved stellar population along the major axis of NGC 4244 to study the age distribution of stars across its break. NGC 4244 is a late-type SAcd spiral galaxy with a maximum rotation speed of about 95 km s^{-1}. We use a distance modulus of 28.20 for NGC 4244, as determined from the tip of the red giant branch (RGB) method by Seth et al. (2005a). The observations and data reduction are described in § 2, the

[1] Space Telescope Science Institute, Baltimore, MD 21218.
[2] Harvard-Smithsonian Center for Astrophysics, Cambridge, MA 02138.
[3] Max-Planck-Institut für Astronomie, D-69117, Heidelberg, Germany.
[4] University of California, Irvine, CA 92697.
[5] Queen's University, Kingston, ON, Canada.
[6] University of Washington, Seattle, WA 98195.
[7] Rice University, Houston, TX 77005.
[8] University of Cambridge, Cambridge CB3 0HA, UK.

DE JONG ET AL.

stellar distributions are investigated in § 3, and we finish with discussion and conclusions in § 4.

2. OBSERVATIONS AND DATA REDUCTION

Our stellar photometry was derived from *Hubble Space Telescope* observations in the F606W and the F814W bands with the Advanced Camera for Surveys (ACS) Wide Field Camera. We obtained SNAP observations with typical total exposure times of about 700 s in each filter split across two exposures. This data set is part of the GHOSTS survey of 14 galaxies with similar data as presented here (de Jong et al. 2007).

We used DOLPHOT (Dolphin 2000) to obtain point-spread function—fitting stellar photometry of our fields. The output of DOLPHOT was filtered to select only real stars using a combination of criteria on signal-to-noise ratio (S/N), magnitude, and DOLPHOT flag and sharpness parameters. These criteria remove most nonstellar objects (galaxies and image defects) while leaving a large fraction (but certainly not all) stellar objects in the sample. Contamination from unresolved galaxies occurs only at low S/N, where a sharpness criterion is too poorly defined to separate all galaxies from stars. At the bright end there may be some Galactic foreground contamination, but this is expected to be less than 10 stars per $3' \times 3'$ ACS field for $m_{\text{F814W}} = 23–26$ mag (Girardi et al. 2005).

We ran DOLPHOT artificial star tests with at least 1 million stars per ACS pointing to calculate incompleteness corrections as a function of stellar magnitude, color, and crowding. Each observed star was given an observing probability based on these artificial star tests, which was used to correct the star count radial profiles described in the next section. The average correction is about 2.5 in the most crowded regions, reducing to less than 1.1 in the outer regions. Full details of the GHOSTS data pipeline will be described in a forthcoming paper (D. J. Radburn-Smith et al. 2007, in preparation).

3. STELLAR DENSITY PROFILES

In Figure 1 we show the color-magnitude diagram for the ACS field at the northeast end of the disk that covers the disk break. Several different stellar evolutionary stages can be identified in this diagram. We have used polygons to identify our separation in broad evolutionary stages, but one should realize that some overlap in age will exist in the different polygons for certain ages and metallicities (see also Seth et al. 2005b).

The magenta polygon indicates the region dominated by stars less than 100 Myr old. The main-sequence stars are on the left. Barely separated from the main sequence at about $m_{\text{F606W}} - m_{\text{F814W}} \sim 0.1$ are the blue He-burning stars. The spur up at about $m_{\text{F606W}} - m_{\text{F814W}} \sim 1.0$ are red He-burning stars. These stars have been partly excluded from this bin, as they overlap with the other populations. We refer to this bin as the young main-sequence (YMS) population. The blue polygon is dominated by older main-sequence and He-burning stars of about 100–300 Myr old (labeled the MS population). The green polygon indicates the region dominated by asymptotic giant branch (AGB) stars of at least 0.3 Gyr, but mostly of intermediate age (1–3 Gyr), with a tail to older ages of up to 10 Gyr. The red polygon is mostly populated by metal-poor RGB stars. Almost all these stars will be older than 5 Gyr. However, even for a constant star formation rate population this polygon is dominated by ~8–12 Gyr old stars, and younger populations can only dominate if star formation was skewed toward younger ages. We use these four population boxes to investigate the spatial distribution of stars of different age.
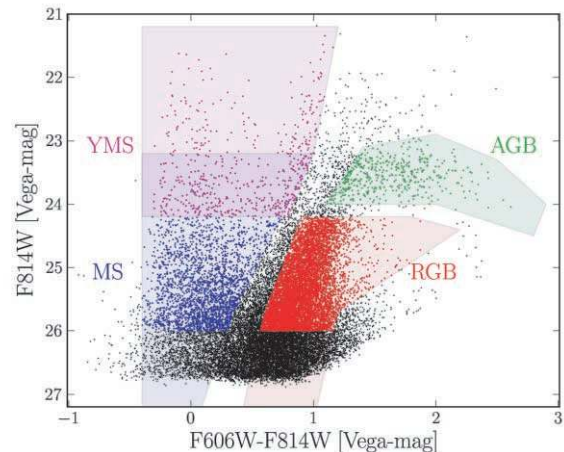

Fig. 1.—Color-magnitude diagram of the ACS field straddling the northeast break of NGC 4244. The colored polygons identify the marked populations. Colored dots show the selected stars, limited to $m_{\text{F814W}} < 25.9$ mag.

In Figure 2 (*bottom*) we show an SDSS image of NGC 4244 with the ACS fields overlaid. Shown in color are five strips used to extract star count profiles. In Figure 2 (*top*) we present the radial star count in these five strips parallel to the major axis for our four population boxes. The contamination-subtracted star counts are presented as symbols with 2 σ Poisson noise error bars. Downward pointing arrows indicate that the Poisson noise would move these points below the contamination level as determined from the average contaminant (Galactic stars, unresolved galaxies, and image defects) density in the outermost major and minor axis fields.

Most conspicuous in the comparison of the different midplane profiles is that they all show a break in their exponential slope at about $-420''$ (-9.0 kpc), independent of stellar population. *Whatever causes this truncation, it affects stars of very different ages in the same way.* The projected scale length in the midplane changes by at least a factor 4 for RGB and AGB stars, and even more so for the young stars, as they have a much larger inner scale length. This flatter distribution for young populations could be caused by star formation mainly occurring in a ring or in wide spiral arms. The radial distribution is not symmetric in both directions—especially for young stars, supporting the aforementioned spiral arm interpretation—and our southwest field is not at a large enough radius to detect the break on that side.

The MS and RGB populations have steep midplane surface density profiles beyond the break, dropping by at least a factor of 600 in 5 kpc. For the YMS and AGB profiles we cannot access the exact behavior across the break because of the much lower counts so that the profiles get lost in the gap between two ACS fields at $-500''$ to $-600''$. However, the upper limits in the outer fields show that a significant break must occur for these populations as well.

The RGB star count profiles agree well with luminosity profiles extracted from the SDSS image, and by lining them up we find that we reach about 31 i_{AB}-mag arcsec^{-2} equivalent surface brightness. Our measurements also agree well with previous integrated light measurements by van der Kruit & Searle (1981) and Fry et al. (1999). These authors find a truncation radius of about $570''$, larger than our $420''$ break radius. However, their truncation measurements are the average of the shorter northeast break radius observed here and the larger
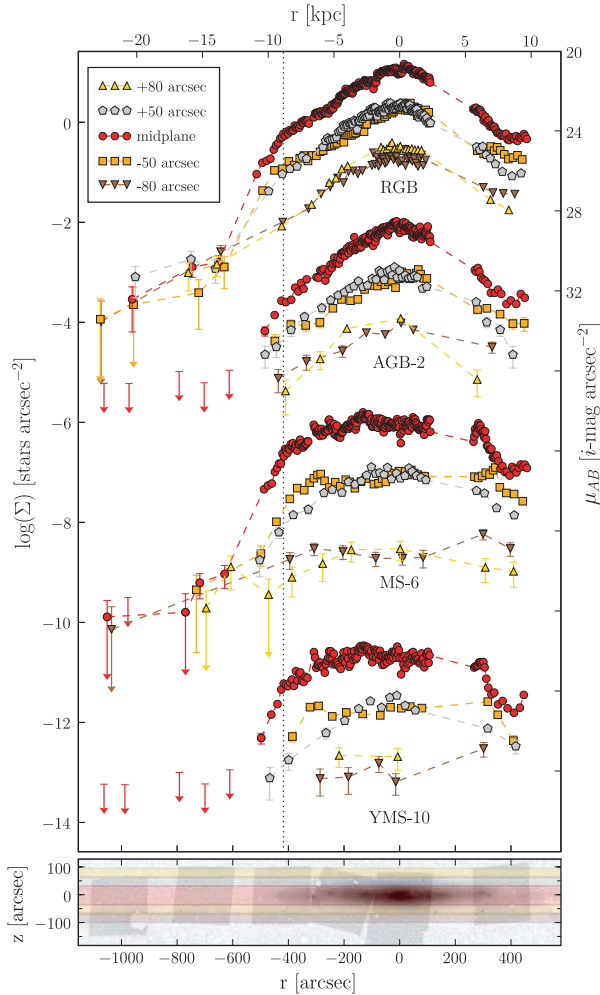
FIG. 2.—*Top*: Incompleteness-corrected star count profiles of NGC 4244. Profiles are shown for a 70″ wide strip along the midplane, and for 35″ wide strips offset 50″ and 80″ above and below the plane, respectively. The different symbols and colors used for the five strips are identified in the inset. Contamination-subtracted star count surface density (Σ) profiles are presented for the four CMD regions identified in Fig. 1 as marked, where for clarity the AGB, MS, and YMS populations have been offset by −2, −6, and −10, respectively, in $\log(\Sigma)$. The error bars are 2 σ Poisson noise uncertainties, with arrows indicating that Poisson uncertainty will move the counts below the background level. The 2 σ upper limits are plotted for bins in which we detect fewer than three stars. For reference we show the equivalent SDSS *i*-band surface brightnesses on the right axis, which was obtained by lining up the SDSS *i*-band integrated light profiles with the RGB stellar density profiles. *Bottom*: SDSS image of NGC 4244 rotated by 42.7°, such that the northeast is to the left. Overlaid are the positions of our ACS fields in gray and the position of the strips used to extract the profiles above, in the same color coding.

southwest break radius, and the edge-on projection of the truncation causes deviations from an exponential profile at radii smaller than the truncation radius.

At about −640″ the MS and RGB star count profiles seem to change scale length again to a shallower slope. This occurs close to our detection limit, and the shape and slope of this outer profile is poorly constrained due to the uncertainty in the contamination level. This might be a diffuse halo, akin to our detection on the minor axis (Seth et al. 2007), as this component shows only marginal concentration toward the midplane.

Figure 2 also highlights the behavior of the break as a function of height above the midplane. Inside the break, the profiles at

each of the vertical offset positions have very similar radial distributions for a given population. The density differences between the different vertical positions are larger for the younger populations due to their shorter scale height (Seth et al. 2005b). The break occurs at roughly the same radius in the 50″ offset profiles as in the midplane profiles. Beyond −420″ the slope of the profile gets shallower because all profiles beyond the break, independent of the height above the disk, converge to the same star count level at about 640″ from the center. At 80″ above and below the disk there is no longer a break visible, as the profile slope beyond the break has become equal to the inner slope.

4. DISCUSSION AND CONCLUSIONS

Our *HST* ACS star count data for NGC 4244 allow us to derive the following observations:

1. The northeast major axis radial star count profiles show a sharp break with two exponential sections. The stellar surface density drops by at least a factor of 600 before reaching a diffuse halo or the background contamination level.

2. The surface density profiles on the major axis for the young, intermediate-age, and old populations all show a break at the same radius.

3. The break occurs at the same radius independent of height above the midplane. The inner scale length is relatively constant, but the outer slope becomes gradually shallower with increasing disk height. This means that in face-on projections the break will be less pronounced.

The observation that all stellar populations, regardless of age, have similar breaks in the midplane profiles puts the strongest constraint on models of break formation, assuming that the NGC 4244 break is representative of other breaks. Most notably, any model where breaks are caused by a sudden change in star formation rate will now have to explain why the radius at which this occurs is stable over a very long time. The model will also have to explain why the breaks in the different populations have similar shapes, whereas one would expect that a very old break would be smoothed by the dynamical heating that we know occurs in older populations.

For instance, a model like that of van der Kruit (1987), in which the break results from the specific angular momentum distribution of a collapsing gaseous sphere that limits the maximum angular momentum available to redistribute gas in the outer disk, has several problems. Over time, more and more gas will decouple from the Hubble flow with different distributions of specific angular momentum, and it is hard to conceive that the cutoff radius would never change. Furthermore, the formation of bars and spiral arms redistributes angular momentum from the central regions to the outer disks so that the current specific angular momentum distribution no longer necessarily reflects the initial distribution (e.g., Debattista et al. 2006). Finally, as the H I gas distribution of many galaxies is significantly more extended than their stellar distribution, it would seem that higher angular momentum gas is often already present (although this is currently not true for NGC 4244; Olling 1996).

Models that rely on some star formation threshold will require fine tuning to keep the threshold at the same location with respect to the broad stellar distribution. Models that rely on the properties of the gas alone (e.g., Schaye [2004] for gas density; Kennicutt [1989] for gas stability) will need to explain why any accreted gas redistributes itself in such a way as to keep the threshold in place for 10 Gyr. It is certainly possible that the gas responds

to the stellar mass already present, as gas flaring and warping seems to indicate (van der Kruit 2007). In NGC 4244, the H I rotation curve drops as the gas density begins to decline, flare, and warp all at about 550″ (Olling 1996), somewhat beyond the break radius. A model that depends on both gas and stellar mass distribution (e.g., Dopita & Ryder 1994) might provide a solution, but still would have a hard time explaining the sharpness of the break in the very old RGB population. Furthermore, all these models may have problems explaining why not all galaxies show breaks (e.g., NGC 300 has an exponential profile over 10 scale lengths; Bland-Hawthorn et al. 2005).

Secular evolution driven by bars and spiral arms can also lead to breaks by redistributing angular momentum and hence stellar mass (e.g., Debattista et al. 2006). This dynamical redistribution of mass will be the same for all age populations. However, if we want to create a break by secular evolution of stars alone, the break must be created on a timescale of less than 100 Myr. When we account for the fact that the gas will also be involved in the secular evolution, we can allow longer timescales, but we then have a similar problem as with the threshold models in that star formation must be proportional to stellar mass density. Furthermore, the secular evolution model requires a significant bar, yet we find no evidence for a strong bar in NGC 4244. Our *Spitzer* 3.6 and 4.5 μm images (B. W. Holwerda et al. 2007, in preparation) show an elongated shape with some twist in the isophotes out to 50″ (one-third of a disk scale length), but we see no vertical thickening. The H I velocity field shows some irregularities between 200″ and 300″ (Olling 1996) that could point to a larger bar, but it is not obviously associated with any features in the optical and IR images. Finally, the factor of 600 decrease in surface density at the break (or ~100 compared to the extended inner exponential disk) makes it unlikely that the break is just a spiral arm seen edge-on. This amplitude of arm-interarm contrasts has never been observed in face-on galaxies.

Tidal stripping by galaxy interactions might be another route for creating galaxy breaks (and antibreaks). This mechanism is only effective after multiple interactions, as in a galaxy cluster environment (Gnedin 2003). This is unlikely to be the case here, as NGC 4244 is the second brightest member of a very loose group with mainly very late-type irregular members, and NGC 4244 has no detected H I companions within 40 kpc (Dahlem et al. 2005).

Disk heating and star stripping by pure dark matter subhalos with a ΛCDM power spectrum is the final model for disk breaks we consider here (Kazantzidis et al. 2007, in preparation). This model has theoretical similarities to the galaxy/cluster interaction model described above, except that the mass-power spectrum of interactions is very different. In this model disk stars are heated by the constant bombardment of dark matter subhalos whizzing through the disk. The original stars in a thin disk will spread into a thicker disk and a diffuse halo develops. At the disk outskirts, where disk self-gravity is low, stars are stripped and a truncation develops. If the stripping occurs quickly, independent of stellar age and scale height, this model might well explain our observations.

The stripped stars would form a diffuse, very flattened halo around the galaxy with streamlike substructure due to the interactions with the dark matter subhalos. This is not unlike the structure we see around NGC 4244, with extended components along the major and minor axis of similar surface densities, which, if present around the whole galaxy, would form a very flattened extension around the disk. Unfortunately, the number of stars detected in the halo of NGC 4244 is too low to measure substructure. Any stellar halo formed through subhalo stripping should not be confused with the stellar halos that form from disrupted satellites in hierarchical galaxy formation. The diffuse halo we detect here is more massive than predicted by these kinds of models for galaxies with masses similar to that of NGC 4244 (Purcell et al. 2007).

It is conceivable that several of the above models are at play simultaneously. To have a sharp, deep factor of 600 break in the old RGB population one likely needs one of the dynamical methods, in which the truncation radius is probably set where the stellar disk self-gravity no longer dominates the potential and where warps are predicted to start (Saha & Jog 2006). Once one of the dynamical methods has created a truncation, later infalling gas will respond to the overall potential in such a way as to set up a star formation threshold at that location. Alternatively, the dynamics of a spiral density wave may interact with a star formation threshold to set a similar feature in the radial profile for young and old stars. Notwithstanding this caveat, dynamical break explanations are favored, as they more naturally explain why profile shapes should be similar for both young and old stars. Analysis of similar GHOSTS data on a large number of galaxies promises to strengthen the constraints on these models.

Facilities: HST(ACS), Sloan

REFERENCES

Bland-Hawthorn, J., et al. 2005, ApJ, 629, 239
Dahlem, M., et al. 2005, A&A, 432, 475
Debattista, V. P., et al. 2006, ApJ, 645, 209
de Jong, R. S., et al. 2007, preprint (astro-ph/0702168v1)
Dolphin, A. E. 2000, PASP, 112, 1383
Dopita, M. A., & Ryder, S. D. 1994, ApJ, 430, 163
Elmegreen, B. G., & Hunter, D. A. 2006, ApJ, 636, 712
Erwin, P., Beckman, J. E., & Pohlen, M. 2005, ApJ, 626, L81
Fall, S. M., & Efstathiou, G. 1980, MNRAS, 193, 189
Fry, A. M., Morrison, H. L., Harding, P., & Boroson, T. A. 1999, AJ, 118, 1209
Girardi, L., et al. 2005, A&A, 436, 895
Gnedin, O. Y. 2003, ApJ, 589, 752
Kazantzidis, S., et al. 2007, preprint (arXiv:0708.1949)
Kennicutt, R. C., Jr. 1989, ApJ, 344, 685
Kregel, M., & van der Kruit, P. C. 2004, MNRAS, 355, 143
Olling, R. P. 1996, AJ, 112, 457

Pérez, I. 2004, A&A, 427, L17
Pohlen, M., Dettmar, R.-J., Lütticke, R., & Aronica, G. 2002, A&A, 392, 807
Pohlen, M., & Trujillo, I. 2006, A&A, 454, 759
Pohlen, M., Zaroubi, S., Peletier, R. F., & Dettmar, R.-J. 2007, MNRAS, 378, 594
Purcell, C. W., Bullock, J. S., & Zentner, A. R. 2007, ApJ, 666, 20
Saha, K., & Jog, C. J. 2006, MNRAS, 367, 1297
Schaye, J. 2004, ApJ, 609, 667
Seth, A., et al. 2007, preprint (astro-ph/0701704v1)
Seth, A. C., Dalcanton, J. J., & de Jong, R. S. 2005a, AJ, 129, 1331
———. 2005b, AJ, 130, 1574
Trujillo, I., & Pohlen, M. 2005, ApJ, 630, L17
van der Kruit, P. C. 1979, A&AS, 38, 15
———. 1987, A&A, 173, 59
———. 2007, A&A, 466, 883
van der Kruit, P. C., & Searle, L. 1981, A&A, 95, 105